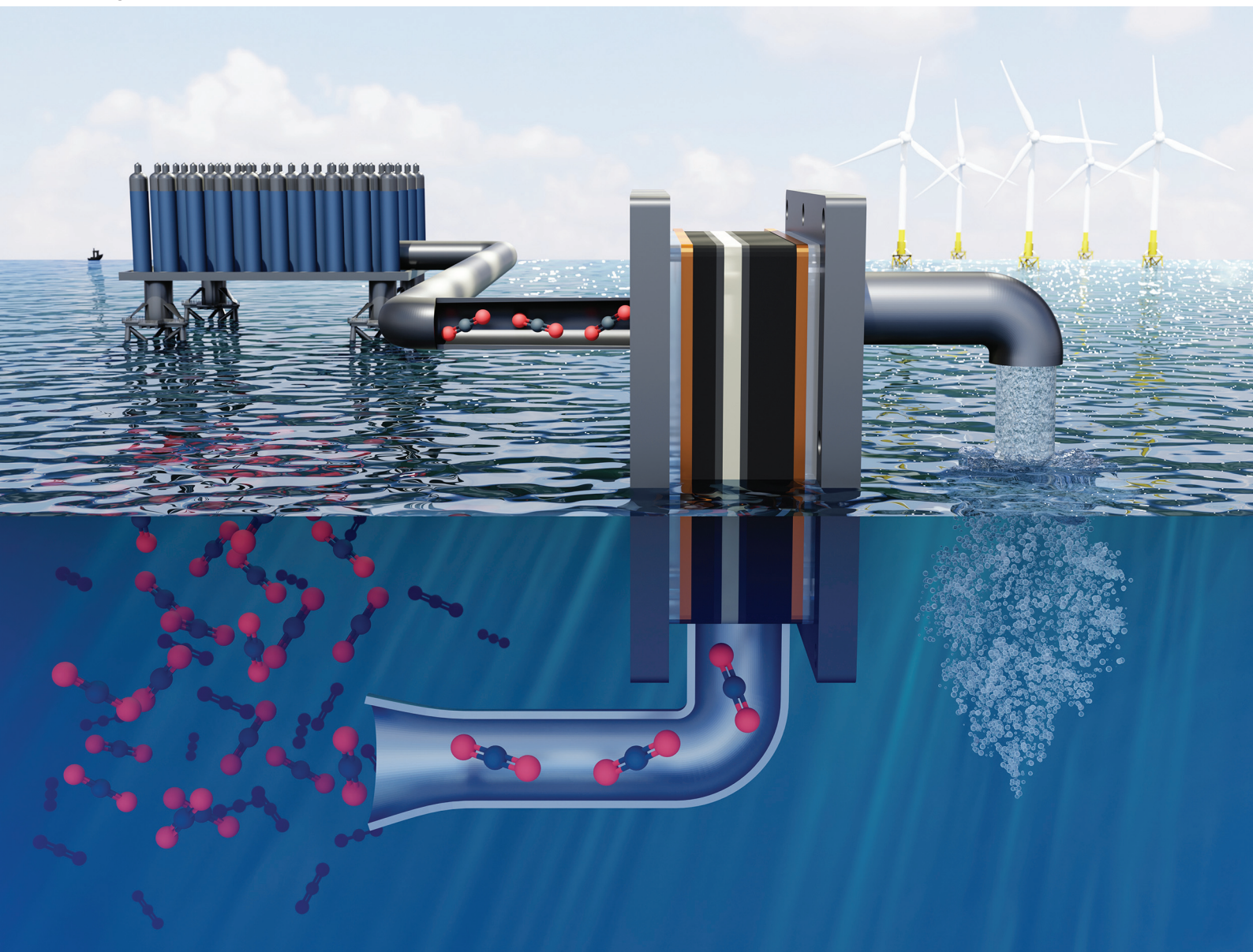


Green Chemistry

Cutting-edge research for a greener sustainable future

rsc.li/greenchem

Volume 27
Number 24
28 June 2025
Pages 6909-7392



ISSN 1463-9262

PAPER



Tom Breugelmans *et al.*
Feasibility study of an electrochemical hydrogen looping
system for indirect ocean capture

PAPER

[View Article Online](#)
[View Journal](#) | [View Issue](#)


Cite this: *Green Chem.*, 2025, **27**, 7137

Feasibility study of an electrochemical hydrogen looping system for indirect ocean capture†

Siebe De Ley,  Sven Arnouts,  Kevin Van Daele,  Jonas Hereijgers and Tom Breugelmans *

Electrochemical hydrogen looping is a recently developed, sustainable technology to address decentralized anthropogenic carbon dioxide emissions by indirectly retrieving CO₂ from oceans. However, various economic and technical challenges such as efficiency and scalability remain, currently inhibiting industrial implementation. Moreover, salt management will be of particular importance as a consequence of the alkaline hydrogen evolution reaction in combination with the ionic seawater content, causing precipitations. This work explored and improved the feasibility of the electrochemical hydrogen looping system by benchmarking the performance using synthetic seawater and, for the first time, realistic seawater, comparing cell voltage, capture efficiency, and electrochemical energy consumption. Using synthetic seawater, a record-low electrochemical energy consumption of 77.5 kJ mol⁻¹ CO₂ was obtained. Transitioning to realistic seawater, enabled us to uncover challenges such as Mg(OH)₂ and Ca(OH)₂ salt precipitation on the cathode and membranes, resulting in a continuously rising cell voltage, impeding long-term operation. Introducing an *in situ* acidic wash step (0.5 M HCl, 45 mL min⁻¹) reduced the voltage increase over a 4-hour operation by 13%, improving long-term stability. Despite membrane scaling challenges, a record-low electrochemical energy consumption of 100.8 kJ mol⁻¹ CO₂ was achieved employing realistic seawater.

Received 5th October 2024,
Accepted 27th March 2025

DOI: 10.1039/d4gc05943c

rsc.li/greenchem

Green foundation

1. The real world feasibility of an electrochemical hydrogen looping (EHL) system was assessed by mapping the challenges that arise when realistic seawater is utilised, for the first time, and a preliminary mitigation strategy was proposed to advance this young technology toward removing CO₂ from the Earth's atmosphere by indirect ocean capture.
2. Here, the electrochemical energy consumption to recover CO₂ from seawater was lowered by 19% from the state-of-the-art. Simultaneously, invaluable insights were gained on the effect of realistic seawater on the EHL system, which had previously solely been tested with synthetic seawater.
3. Further research should focus on elevating the operating current density toward more industrially relevant values, as well as investigating a more sustainable mitigation strategy. The latter currently consists out of an acidic wash step, which should ideally be eliminated in future research.

1. Introduction

The increasing urgency of global warming has intensified efforts to reduce carbon dioxide (CO₂) emissions, with carbon capture and storage (CCS) or – utilization (CCU) technologies

emerging as key solutions.^{1–3} These approaches pursue the reduction of anthropogenic CO₂ emissions, which is crucial to meet the Paris Agreement goals.^{4–7} Among the various carbon capture methods, capturing CO₂ directly from industrial point sources or indirectly from natural carbon sinks like the atmosphere^{8–10} and oceans^{11,12} offer distinct benefits. Next to direct air capture (DAC), which is currently being piloted to remove 4000 tons of CO₂ annually, indirect ocean capture provides several advantages.^{13,14} This approach represents a promising alternative to DAC due to the higher volumetric concentration of CO₂ in seawater, which is approximately 140 times higher than in the Earth's atmosphere.^{15,16} Oceans also serve as a vast carbon reservoir with natural sequestration capabilities. While the atmosphere's overall volume is larger, the oceans contain about 50 times more CO₂, making it the largest

Applied Electrochemistry and Catalysis (ELCAT), University of Antwerp, 2610 Wilrijk, Belgium. E-mail: Tom.Breugelmans@uantwerpen.be, Siebe.DeLey@uantwerpen.be, Sven.Arnouts@uantwerpen.be, Kevin.VanDaele@uantwerpen.be, Jonas.Hereijgers@uantwerpen.be; <https://elcat.be/>

† Electronic supplementary information (ESI) available: Bjerrum plot of the fraction DIC in SSW; comparison of other carbon capture technologies; calculations of theoretical cell potentials of all indirect ocean capture technologies; EEC calculation; capture efficiency calculation; SEM EDS of the NaEM from the side facing the middle compartment; images of salt precipitation issues. See DOI: <https://doi.org/10.1039/d4gc05943c>

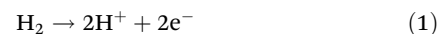
natural CO₂ sink.^{15,17} When optimized, indirect ocean capture has the potential to remove gigatons of CO₂ per year, which could significantly help in mitigating climate change. Additionally, this method addresses ocean acidification by reducing the CO₂ content in seawater, potentially helping to restore the marine pH balance and support biodiversity in ocean ecosystems.¹⁸

Electrochemical oceanic carbon capture has been identified as a promising decarbonization route in which several approaches are being explored, including electrochemical hydrogen looping (EHL),¹⁹ bipolar membrane electrodialysis (BPMED),²⁰ and electrolytic cation exchange modules (E-CEM).²¹ Provided that these methods are powered by renewable energy sources, they could support a sustainable future by decarbonizing seawater without significant environmental impact. However, technical and economic challenges remain for transposing these technologies toward industrial levels, including issues such as salt precipitation, membrane fouling, and high costs associated with energy and materials.^{22–24}

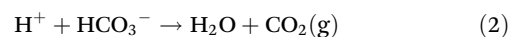
While BPMED and E-CEM technologies have already been thoroughly explored,^{25,26} the EHL system (Fig. 1) is relatively new and uninvestigated since it was first reported by Yan *et al.* in 2022.¹⁹ Additionally, it has a lower theoretical cell voltage (0.48 V) than BPMED (0.83 V) and E-CEM (1.73 V) and a record low energy consumption for CO₂ removal from synthetic seawater (SSW) requiring 660 kW h per ton CO₂ was achieved.¹⁹ The EHL system operates on the same principle of pH swing as BPMED and E-CEM, targeting an acidified seawater stream to extract CO₂ from seawater (Fig. S1†). However, instead of the oxygen evolution reaction (OER), EHL uses the hydrogen oxidation reactions (HOR) at the anode (eqn (1)). This produces protons that acidify the seawater in the central compartment, releasing CO₂ for capture (eqn (2)). At the cathode, the hydro-

gen evolution reaction (HER) generates hydroxyl ions, creating a basic solution (eqn (3)). Finally, these acidified and basified seawater streams can be combined to form a slightly alkaline solution suitable for ocean discharge.²⁷

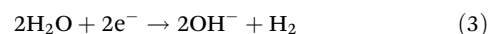
Anode:



Center compartment:



Cathode:



Furthermore, the EHL process theoretically creates a self-sustaining system by circulating hydrogen generated at the cathode back to the anode for continuous use, thereby minimizing material consumption. Additionally, the system maintains charge neutrality by transporting sodium ions to the cathode, where they react with hydroxyl ions to form sodium hydroxide, further increasing the alkalinity of the discharge stream. When fully scaled, EHL offers an efficient, cost-effective option for indirect ocean capture, addressing both decentralized CO₂ emissions and ocean acidification.

In the present study, an EHL system was developed to enhance the performance and to examine its real world feasibility by optimizing the electrochemical energy consumption (EEC) under various conditions, such as current density and seawater flow rate. Moreover, this approach was tested for the first time with realistic seawater (RSW), containing all naturally occurring ions. The system demonstrated an optimal energy consumption of 536 kWh per ton of CO₂ with synthetic seawater, an improvement of 19% over previously reported values. With realistic seawater, the energy consumption was 636 kWh per ton of CO₂, which remains comparable to more established capture technologies as shown in Table S1.† However, prolonged use with RSW revealed several challenges, particularly salt precipitation caused by reactions between hydroxyl ions and minerals like magnesium and calcium. To address this, a preliminary *in situ* acidic wash step was introduced to prevent fouling and salt buildup, allowing the system to maintain its record-low efficiency over an extended operation of 10 hours. These results indicate that mitigating the inherent salt precipitation and membrane scaling are crucial for this young technology to become industrially feasible, operating at high current densities with real world seawater.

2. Materials & methods

Synthetic seawater (SSW), was prepared by dissolving sodium chloride (99.5%, for analysis, Thermo Scientific, Denmark) and sodium hydrogen carbonate (99.7+%, Chem-Lab, Belgium) in ultrapure water (Milli-Q, resistivity 18.2 MΩ cm, Millipore, USA) to obtain concentrations of respectively 0.5 M and 2.5 mM.

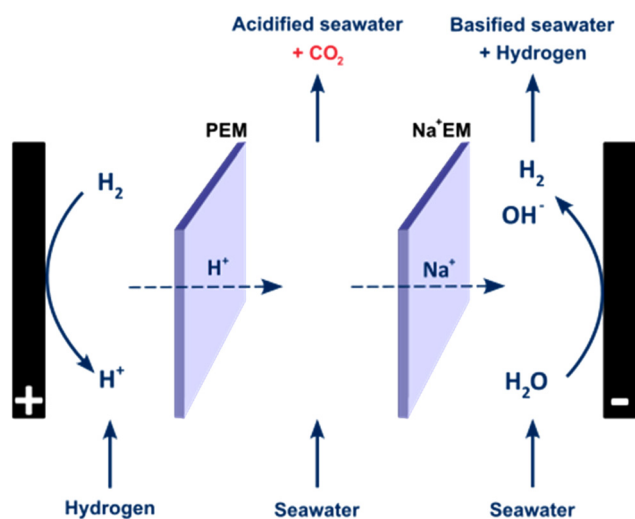


Fig. 1 Schematic overview and principle of the EHL flow cell for indirect ocean capture.

Realistic seawater (RSW) was prepared from a seawater concentrate (Absolute ocean, ATI-Aquaristik, Germany) which was diluted to the right concentration (12 vol% concentrate) in ultrapure water.

The **washing agent** in this research was 0.5 M hydrochloric acid (37%, Thermo Fisher Scientific, Belgium).

The **Anode catalyst ink** was prepared by mixing Pt/C nanopowder (platinum, nominally 20% on carbon black, powder, Thermo Scientific, Germany) with a Nafion dispersion (D520, 5% w/w in water and 1-propanol, AlfaAesar, Belgium) as binder so that a mass ratio of catalyst to binder of 85/15 was obtained. Thereafter, ultrapure water and isopropanol (99.8%, Chem-lab, Belgium) were added in a 40/60 volume ratio, before sonication (NexTgen Lab120) for 30 minutes at 34 kHz and an 84 μm amplitude.

Gas diffusion electrodes (GDEs) with dimensions of 4 by 4 cm (16 cm^2 geometrical active surface area) were made by spray coating the above mentioned anode catalyst ink upon the microporous layer of a carbon paper (Sigracet GDL 39 BB, Ion Power, Germany) using an airbrush (FE-186K, Fengda, Airgoo Pneumatic, The Netherlands) fitted with a 0.5 mm nozzle, employing argon (99.999%, Air Liquide, Belgium) as carrier gas. During this process, the GDE was fixed on a hot plate at 70 $^{\circ}\text{C}$ to evaporate the ink's liquids and deposit the catalyst particles. The GDE loading was aimed at 2.5 mg cm^{-2} which was verified by weighing the GDE before and after spray coating.

The **electrochemical reactor** is a three-compartment cell used at ambient conditions. The anode consists of a graphite plate holding the GDE, pressed against a pretreated NafionTM 117 (Ion power, Germany) proton exchange membrane (PEM). The pretreatment consists of four consecutive steps which are conducted in the following order: boiling the membrane in (I) 3% H_2O_2 (hydrogen peroxide, 30%, VWR Chemicals, France), (II) ultrapure water, (III) 0.75 M H_2SO_4 (sulfuric acid, 95–97%, Honeywell, Belgium) and (IV) ultrapure water for one hour each. The middle compartment is a 3D-printed plate that creates a spacing of 5.4 mm and supports both membranes bordering this open space. The cathode is a graphite plate that presses a platinum gauze (52 mesh woven from a 0.1 mm diameter wire, 99.9%, Thermo Scientific Chemicals, Belgium) against a sodium exchange membrane, which is obtained by soaking an activated NafionTM 117 in 3 M NaCl (99.5%, for analysis, Thermo Scientific, Denmark) for two days. The platinum gauze was chosen to aim for improved bubble removal, as in a previous study a GDE was employed as the cathode substrate.¹⁹ The graphite plates of both the anode and the cathodic compartment are in contact with copper plate current collectors. All these reactor parts are fixated between two PMMA insulators and aluminum backplates to construct the electrochemical cell, which was torqued at 5 Nm. Fig. 2 illustrates a schematic overview of the experimental setup in which the experiments were conducted. The anode compartment was fed with 5% H_2 in Ar (Air liquide, Belgium) at approximately 100 mL min^{-1} , regulated *via* a Matheson flow meter (FM-1050, Matheson, US). All electrolytes were pumped through the cell

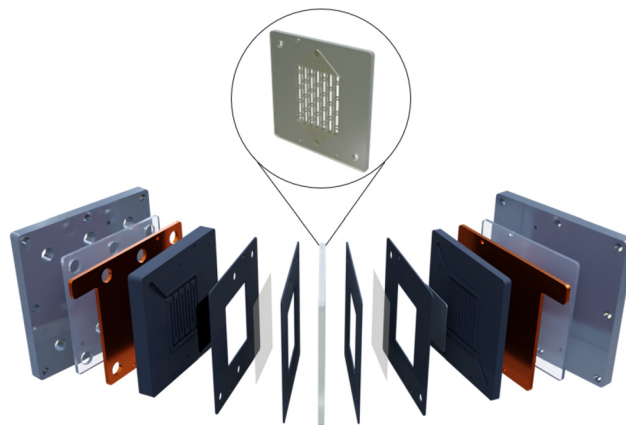


Fig. 2 Exploded view of the in-house manufactured and engineered EHL reactor highlighting the 3D printed middle compartment. The components which make up the reactor are from left to right: endplate; insulating plate; current collector; anodic bipolar plate; carbon GDE; gasket; PEM; gasket; 3D printed middle compartment with supporting structure for the membranes; gasket; NaEM; gasket; Pt gauze; cathodic bipolar plate; current collector; insulating plate; endplate.

at flowrates varying from 15 to 35 mL min^{-1} (1.37 to 3.2 mm s^{-1}) with a peristaltic pump (Shenzhen LabV1, Drifton, Denmark). To release the carbon dioxide in the middle compartment and basify the cathodic compartment, chronopotentiometry was carried out at current densities ranging from 1 to 9 mA cm^{-2} , with a power source (Bi-directional DC power supply, ITECH Electronic, USA).

Sample analysis was performed by measuring the synthetic seawater's pH (LL-Electrode Plus WOC, Metrohm, Belgium) to indicate the carbon content left in the sample (Fig. S1†). For confirmation, the total inorganic carbon (TIC) content was measured to establish the analysis method necessary for realistic seawater. Therefore, a 225 mL sample was taken and sparged with nitrogen (Air Liquide, Belgium) for 12 minutes to remove the dissolved CO_2 . After removal of the gaseous content in the sample, TIC measurements were performed with a TOC analyzer (TOC-L CPH + TNM-L, Shimadzu, Belgium).

Scanning electron microscopy (SEM) measurements were performed using a Thermo Fisher Scientific Quanta FEG 250 microscope operated at 20 kV. Energy dispersive X-ray spectroscopy (EDS) spectra and elemental maps were acquired using the X-MAX^N detector (Oxford instruments) in combination with the Aztec software (v2.1a).

3. Results & discussion

In order to benchmark and compare the experimental results and EHL performance to previously published research, the EHL system was first operated using synthetic seawater (SSW) as electrolyte in the middle and cathodic compartment. The small theoretical potential difference (0.48 V) between the

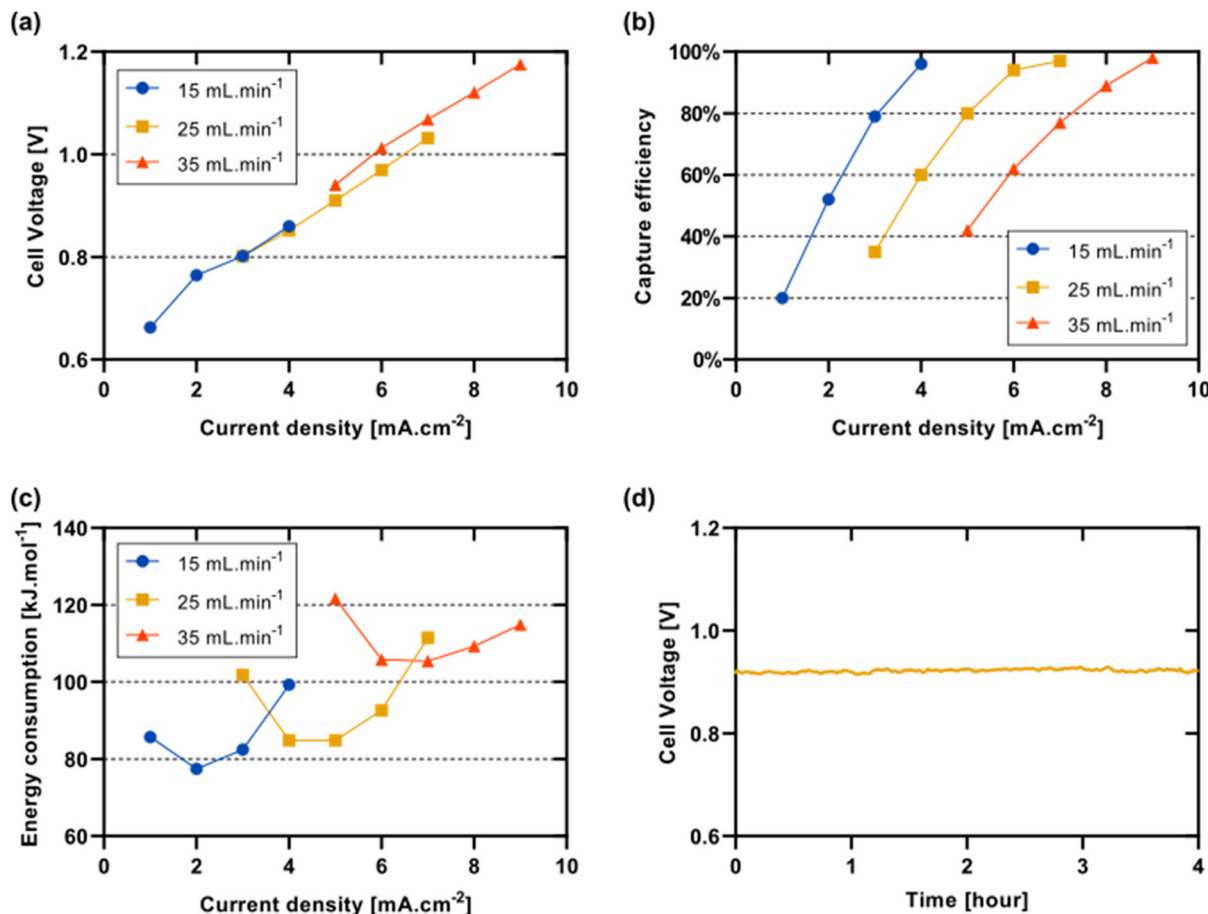


Fig. 3 (a) Cell voltage profile of the EHL reactor at three different SSW flow rates and varying current densities; (b) capture efficiencies of the EHL reactor at three different SSW flow rates and varying current densities; (c) electrochemical energy consumption of the EHL reactor at three different SSW flow rates and varying current densities; and (d) cell voltage response of a four hour experiment with a SSW flow rate of 25 mL min^{-1} and a current density of 5 mA cm^{-2} . For (a), (b) and (c) all data points are the result of one hour experiments of which the mean value is shown on the graphs.

HOR and HER in the acidic and alkaline solution, respectively, combined with the fast kinetics of both reactions led to cell voltages below 1.2 V when operating the flow cell. Fig. 3 shows the performance of the EHL flow cell under different operating conditions, varying current density and SSW flow rate in both liquid compartments during one hour experiments to obtain the optimal operating parameters. Fig. 3a depicts the dependency of cell voltage as function of current density for three different electrolyte flowrates, *i.e.* 15, 25 and 35 mL min^{-1} . Here, it is clear that, as expected, cell voltage increases with current density, but the influence of the flow rate hereon is negligible. Previously, Yan *et al.* reported a decrease in cell voltage with increasing flow rate.¹⁹ However, this reactor configuration does not show a similar effect since a platinum gauze is used as cathode material, instead of a carbon GDE, which allows for better bubble removal even at low flow rates. As a result, all flow rates show similar resistance profiles and there are no significant benefits concerning cell voltage to increase the electrolyte flow rate. Capture efficiencies corresponding to the previously discussed experiments are calcu-

lated according to eqn (4) through TIC measurements and shown in Fig. 3b. These results show an increased capture efficiency with an increasing current density, as more protons are supplied to the SSW in the middle compartment. A logarithmic trend is obtained as this metric is determined by the pH of the outgoing seawater stream, which also utilizes a logarithmic scale. The curves recorded at the three different flow rates are similar as this parameter is determined by the charge per volume. Consequently, the lowest occupied flow rate requires a lower current density to achieve a capture efficiency above 80%, while the higher employed flow rates need a higher current density to reach the same capture efficiency, as demonstrated in Fig. 3b. A capture efficiency as high as 98% was achieved at a flow rate of 35 mL min^{-1} and a current density of 9 mA cm^{-2} . From this the electrochemical energy consumption (EEC) can be calculated, which corresponds to the amount of energy needed for the electrochemical process to capture one mole of CO_2 . The formula for the EEC is given in eqn (5), with I the current, E_{cell} the cell voltage, t the time, Q the volumetric flow rate of the seawater, C the concentration of

CO₂ in the seawater and η the previously calculated capture efficiency.

$$\eta = \frac{C_{\text{Carbon before acidification}} - C_{\text{Carbon after acidification}}}{C_{\text{Carbon before acidification}}} \quad (4)$$

$$\text{EEC} = \frac{I \cdot E_{\text{cell}} \cdot t}{Q \cdot t \cdot C \cdot \eta} \quad (5)$$

The resulting EECs for all experimental conditions are depicted in Fig. 3c, with the lowest recorded value being 77.5 kJ mol⁻¹ CO₂, when operating at a current density of 2 mA cm⁻² and a flow rate of 15 mL min⁻¹, outperforming the lowest reported energy consumption of Yan *et al.* by 25% and the BPMED-2 system, investigated by Digdaya *et al.*, by more than 49%.^{19,28} The former reported 104 kJ mol⁻¹ CO₂ for their EHL system utilizing SSW, while the latter reported a minimal energy consumption of 155.4 kJ mol⁻¹ CO₂ for their improved BPMED system, employing a reversible ferricyanide/ferrocyanide redox couple.²⁸ In addition to improving the EEC due to

efficient bubble removal, the system has proven to be a stable configuration with a stable cell voltage response for four hours of testing with SSW, as shown in Fig. 3d.

After optimizing the performance and ensuring stable operation of the system using SSW, the feasibility of the EHL flow cell was investigated using realistic seawater (RSW). To this end, a seawater flow rate of 25 mL min⁻¹ was selected as this flow rate yielded the lowest EEC for a targeted capture efficiency above 80%. A comparison between the results from the experiments conducted with SSW and RSW, as a function of current density, is shown in Fig. 4.

Fig. 4a illustrates the cell voltage response of the EHL system when either SSW or RSW was used as electrolyte in both the middle and cathodic compartment. Relative to the experiments with SSW, the RSW cell voltage was 9% higher on average after one hour of operation. Moreover, using RSW the cell voltage was not stable over the course of the experiment, but increased over time (first hour of Fig. 4d), contrary to the experiments with SSW. Although, only a minimal loss in

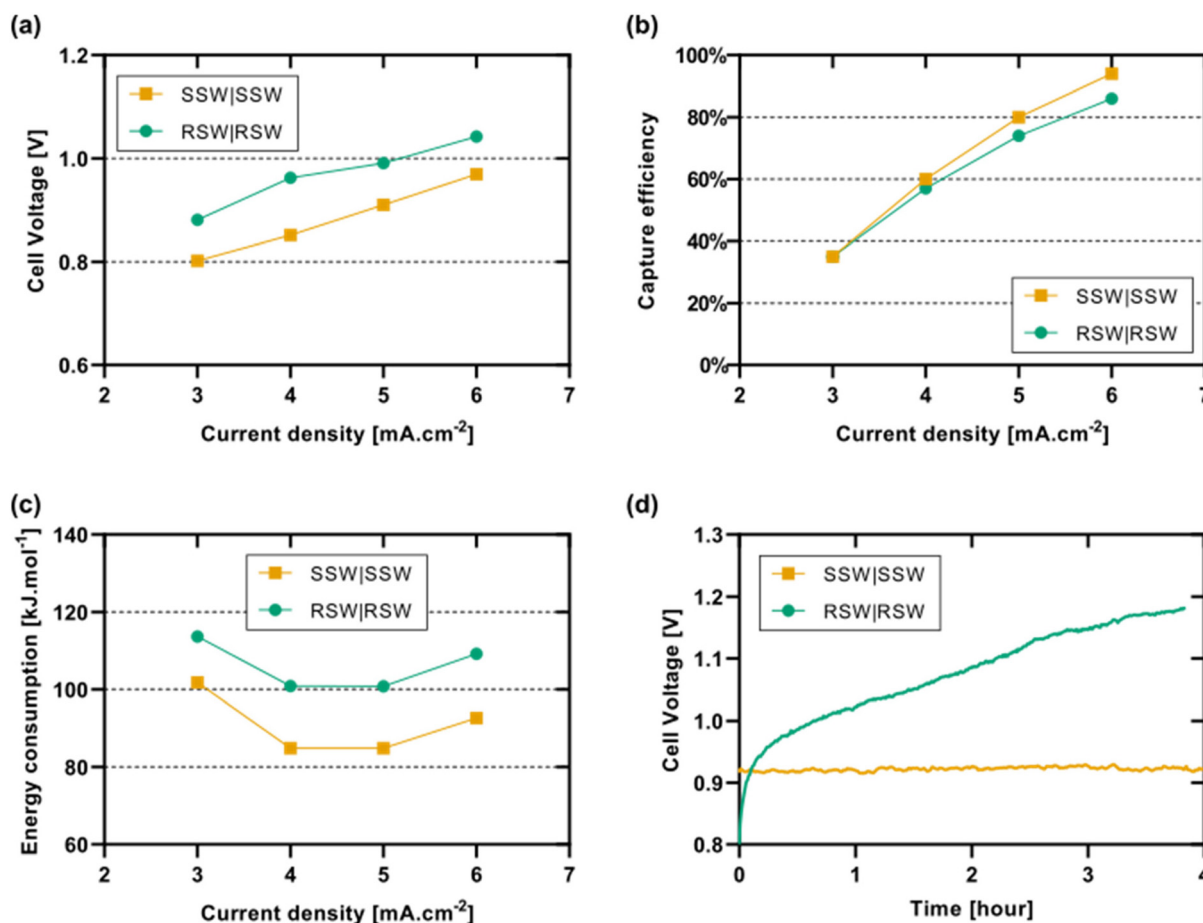


Fig. 4 (a) Cell Voltage profile of the EHL reactor comparing SSW and RSW as an electrolyte in both the middle- and cathodic compartment at varying current densities; (b) capture efficiencies of the EHL reactor comparing SSW and RSW as an electrolyte in both the middle- and cathodic compartment at varying current densities; (c) electrochemical energy consumption of the EHL reactor comparing SSW and RSW as an electrolyte in both the middle- and cathodic compartment at varying current densities; (d) cell voltage response of a four hour experiment with RSW at a current density of 5 mA cm⁻². All experiments were carried out with a seawater flow rate of 25 mL min⁻¹ and all data points in (a), (b) and (c) are the result of one hour experiments of which the mean value is shown on the graphs.

capture efficiency is observed going from SSW to RSW (Fig. 4b), the elevated cell voltages for RSW resulted in an average $15 \text{ kJ mol}^{-1} \text{ CO}_2$ increased EEC for RSW compared to SSW (Fig. 4c). However, it is important to note that the lowest recorded energy consumption for RSW was $100.8 \text{ kJ mol}^{-1} \text{ CO}_2$ at 5 mA cm^{-2} , which is still an improvement on the previously reported minimal value for a one hour experiment with SSW by Yan *et al.*¹⁹ Fig. 4d shows the rise in cell voltage which was exemplified even more during a four-hour experiment using a flow rate of 25 mL min^{-1} and a current density of 5 mA cm^{-2} .

The increasing cell voltage is a direct consequence of the use of RSW, which contains Mg^{2+} and Ca^{2+} ions that precipitate in the form of their hydroxide salts in alkaline conditions. Since the cathodic HER (eqn (3)) produces hydroxyl ions, this salt precipitation is inherently connected to the EHL system in combination with RSW and could pose a real obstruction for this technology regarding industrial applicability. Therefore, we looked into a mitigation strategy to tackle this salt precipitation and further improve the EHL system. Moreover, an *in situ* mitigation strategy was opted, preventing the use of expensive antiscalants.

When RSW is pumped through the alkaline compartment (cathode), where hydroxyl ions are continuously being produced, $\text{Mg}(\text{OH})_2$ and $\text{Ca}(\text{OH})_2$ precipitate on the cathode surface, thereby blocking parts of the active surface area and, consequently, increasing the cell resistance, as shown in Fig. 4d. This precipitation was also visually observed in the flow channels of the cathodic bipolar plate and on the cathode after four hours of continuous operation (Fig. S3a†). Pushing the runtime beyond four hours without any mitigation would lead to the total obstruction of flow in the cathodic chamber. However, salt formation in the cathodic compartment appeared to be not the sole cause of the increasing cell voltage. Membrane scaling resulting from the same mechanism of salt formation was hypothesized to pose an equally big problem. Since the EHL configuration employs cation exchange membranes (CEM), Mg^{2+} and Ca^{2+} ions are transported through the membrane under the electrostatic force generated by the negatively charged cathode. Even though the CEM received a pretreatment to predominantly transport Na^+ ions, this phenomenon is unavoidable when using Nafion™ membranes.²⁹ Moreover, these membranes are known not to be completely permselective, resulting in hydroxyl ions being transported in the opposite direction due to the electrostatic force driving them towards the positively charged anode.³⁰ As a result, hydroxyl ions come in contact with Mg^{2+} and Ca^{2+} ions inside the membrane and at both surfaces of the membrane where they are able to precipitate as salt on the surface or in the membrane's inner structure, a phenomenon typically referred to as membrane scaling.³¹ Consequently, transport pathways through the membrane are blocked over time, contributing to the steadily increasing cell voltage. This phenomenon was also visually observed on the membrane surface after 4 hours of operation (Fig. S3b†).

To confirm this observation of membrane crossover, various experiments were carried out during which RSW was

only cycled through one compartment, this being either the middle or the cathodic compartment. SSW, which contains no Mg^{2+} or Ca^{2+} ions was utilized as electrolyte in the other compartment. Fig. 5 shows the cell voltages during the first 4 hours of operation of each of the cases (SSW|SSW, SSW|RSW, RSW|SSW, RSW|RSW). In the instance where RSW was used solely in the cathodic compartment (Fig. 5, blue curve, SSW|RSW), salt precipitation only occurred on the cathode itself, since in this scenario there are no Mg^{2+} and Ca^{2+} ions present in the middle compartment and consequently there is no flux of these ions from the middle compartment through the membrane towards the cathode. This resulted in a sharp rise of the cell voltage during the first one and a half hours of operation, after which it stabilized, as the cathode was completely saturated with salt. From this point on, the additional salt formation clogged the underlying flow field which had no direct influence on the cell voltage, until it would eventually block the entire electrolyte flow if the experiment was continued for more than four hours. When the use of RSW is limited to the middle compartment (RSW|SSW), no visual salt precipitation was observed on the cathode after four hours of chronopotentiometry. This resulted in a continuously rising cell voltage (Fig. 5, pink curve, RSW|SSW), predominantly caused by membrane scaling. Seeing as the continuously rising cell potential is almost identical to the experiment in which both compartments hold RSW, we concluded that membrane scaling has the largest contribution to the unstable cell potential and, therefore, poses the biggest challenge in terms of long-term operation and EEC.

To confirm the hypothesis of membrane scaling, both pristine and membranes used in the cell during operation with RSW were imaged using scanning electron microscopy (SEM), and complementary energy dispersive X-ray spectroscopy (EDS)

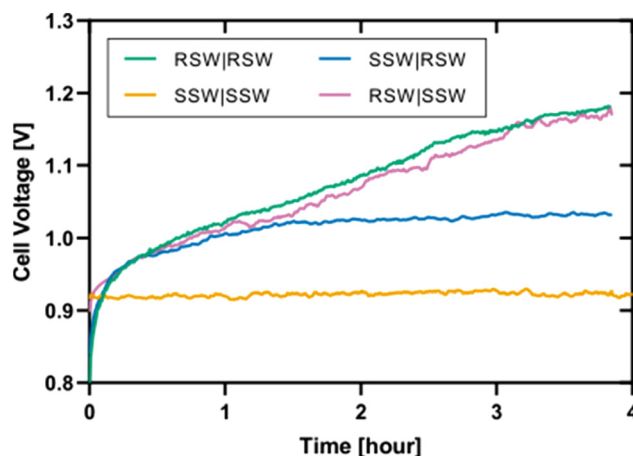


Fig. 5 Cell voltage response of four hour experiments with different electrolytes to unravel the different effects of salt precipitation on the cathode (blue curve) and membrane scaling (pink curve). Legend labels signify the types of seawater used in the middle (middle compartment flow...) and cathodic compartment (...|cathodic compartment flow). All experiments were conducted at a current density of 5 mA cm^{-2} and with a flow rate of 25 mL min^{-1} .

measurements. Fig. 7a and b show the electron images of a pristine and a used NafionTM 117 membrane (membrane side facing the cathodic compartment), respectively, together with the EDS spectra and elemental maps for magnesium, calcium and fluor, a main component in NafionTM CEMs. While the images show no contamination on the pristine membrane, the used membrane clearly shows contamination of Mg and Ca, visible in not only the electron image, but also in the elemental maps. It is important to note, however, that this only confirms scaling of the surface layer of the membrane as the penetration dept of the electrons is only about 5 μm , while the membranes have a thickness of 183 μm . Nonetheless, it can be assumed that the inner membrane is also scaled since also the side facing the middle compartment shows contamination of Mg and Ca (Fig. S2a†) and this can only be attributed by the transport of Mg and Ca through the membrane as these ions are only available in RSW that was only present in the cathodic compartment.

Fig. 5 clearly indicates the necessity of a mitigation strategy to counter the salt precipitation to operate the EHL system for a longer duration. To this extent, the effectiveness of an *in situ* acidic wash step with HCl (variable concentration, *vide infra*) was investigated to regenerate the transport capacity of the membranes and clearing the cathode by re-dissolving the Mg(OH)₂ and Ca(OH)₂ salts. A wash step, which lasted 10 minutes, was introduced after every 50 minutes of continuous operation. During these 10 minutes, an HCl solution was flowed through both the middle and the cathodic compartment for eight minutes at OCV, after which both compartments were thoroughly rinsed using MiliQ for two minutes to remove any acid or salt residues, before reintroducing the RSW and applying a current density of 5 mA cm⁻². To optimize this wash step, the influence of the volumetric flow rate and the concentration of the acid solution during the wash step was investigated to distinguish the importance of increased mass transfer over the amount of supplied acid. Keeping the total amount of hydrochloric acid passing through each compartment constant per wash cycle resulted in the utilization of 0.18 moles of HCl. Consequently, the concentration of HCl was varied from 0.9 M to 0.64 M and finally 0.5 M, which corresponds to flow rates of 25 mL min⁻¹, 35 mL min⁻¹ and 45 mL min⁻¹, respectively. The resulting cell voltages during four hours of operation for each of these wash steps are compared to the original situation before the introduction of an *in situ* wash step and are depicted in Fig. 6.

From Fig. 6, it is immediately apparent that by introducing an *in situ* wash step the cell voltage was lowered by 9.5% with a wash step of 25 mL min⁻¹ with 0.9 M HCl after four hours of operation, compared to no mitigation. At 0.5 M and 45 mL min⁻¹ the improvement in cell voltage over four hours is 13% relative to the original situation without any mitigation. Additionally, taking the voltage recorded after one hour of continuous operation as a reference, the cell voltage, without mitigation, showed an increase of 14.2% over the next three hours. By introducing the *in situ* acidic wash step, we managed to reduce this to 1.6% at the end of the fourth cycle.

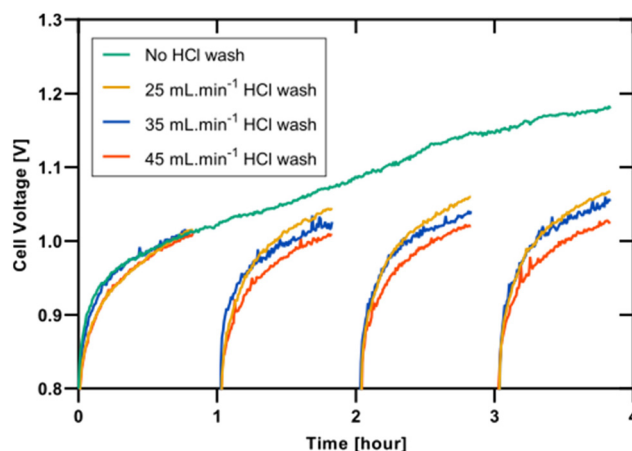


Fig. 6 Cell voltage response of various four hour experiments with a RSW flow rate of 25 mL min⁻¹ and a current density of 5 mA cm⁻². An acidic wash steps is introduced every hour as a mitigation strategy. The HCl wash step is carried out at different flow rates and with varying HCl concentrations: 25 mL min⁻¹ with 0.9 M HCl; 35 mL min⁻¹ with 0.64 M HCl; 45 mL min⁻¹ with 0.5 M HCl.

In order to further validate the effectiveness of the acidic wash step mitigation, used membranes were imaged *via* SEM EDS immediately after operation. Fig. 7c shows the secondary electron image (SEI) and corresponding EDS spectrum and elemental maps for Mg, Ca and F of a membrane washed under the aforementioned ideal conditions. The SEI shows no contamination on the membrane surface after a wash step. However, the EDS spectrum shows peaks for Mg and Ca. This is in accordance with the cell voltage response, which still slightly increases over time during the 50 minutes chronopotentiometry, indicating residual membrane scaling. Nonetheless, it is clear that the peaks in the spectrum of Fig. 7b are far more prominent compared to those in Fig. 7c and membrane scaling has largely been mitigated by introducing an *in situ* acidic wash step.

To further explore the feasibility of the EHL system, 10 hours experiments were conducted to assess membrane scaling and the proposed mitigation strategy. Fig. 8 shows the cell voltage response combined with the EEC of each individual one hour cycle. The rate of increasing cell voltage remained constant over a 10 hours period, which indicates a stable, reduced membrane scaling. The increase in cell voltage was limited to 0.106 ± 0.004 V, demonstrating the effectiveness of the wash cycles. Notably, our EHL displayed an average EEC of 97.8 kJ mol⁻¹, outperforming the best reported value in literature for SSW by 6%. Finally, further optimization in terms of volumetric flow rate, acid concentration, wash step duration and cycle frequency are possible to further lower the EEC and optimize the EHL system performance to improve industrial feasibility.

This research improves upon the work of Yan *et al.* who pioneered the electrochemical hydrogen looping system for indirect oceanic carbon capture, based on the principles of hydrogen oxidation and reduction.¹⁹ In the EHL system, a seawater

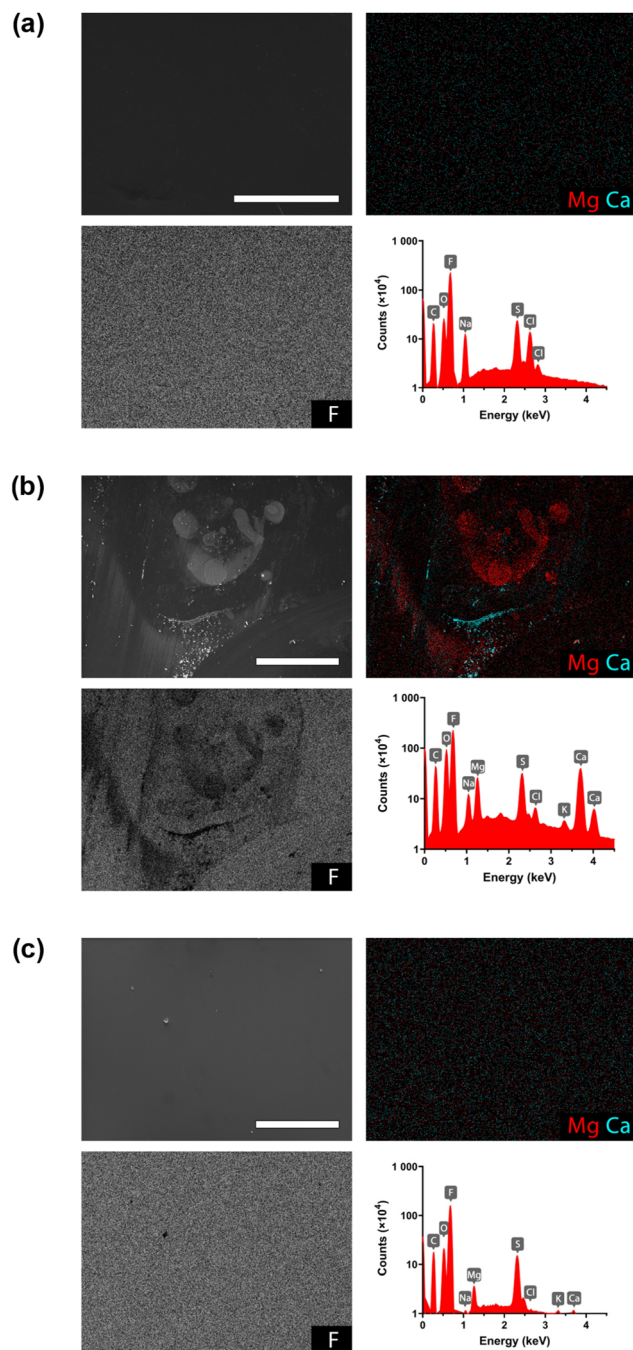


Fig. 7 Secondary electron images, elemental maps and EDS spectra of (a) a pristine Nafion™ 117 membrane, (b) a Nafion™ 117 membrane imaged from the side of the cathodic compartment after 4 hours of operation without washing steps (c) a Nafion™ 117 membrane imaged from the side of the cathodic compartment after four hours of operation including wash steps under the optimal conditions. All scale bars correspond to 250 μm . Experiments with these membranes were carried out at 5 mA cm^{-2} and with a flow rate of 25 mL min^{-1} .

stream undergoes acidification, facilitating the conversion of bicarbonate into CO_2 , by means of a pH swing, which is subsequently captured. This mechanism established EHL as an effective approach for indirect ocean capture of decentralized

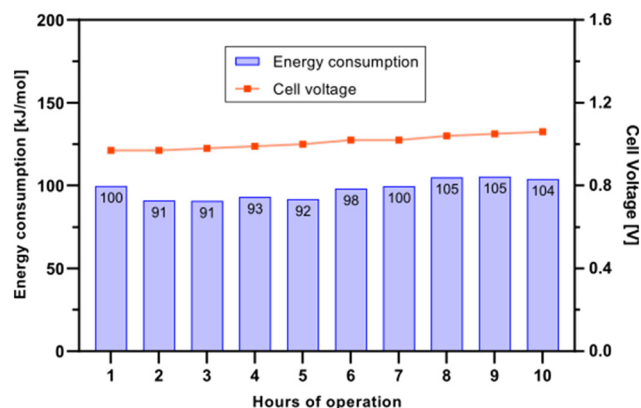


Fig. 8 Cell voltage response and electrochemical energy consumption of a 10 hours measurement with a RSW flow rate of 25 mL min^{-1} and a current density of 5 mA cm^{-2} while introducing a 0.5 M HCl wash step every hour for 8 minutes with a flow rate of 45 mL min^{-1} .

CO_2 emissions, while simultaneously combating ocean acidification.

A comparison of the presented findings with the previous state-of-the-art by Yan *et al.* demonstrates that the EHL flow cell developed in this study is able to recover CO_2 from realistic seawater with a significantly lower electrochemical energy consumption, thereby increasing the green advancement of this young technology. Yan *et al.* reported an EEC as low as 104 $\text{kJ mol}^{-1} \text{CO}_2$ with stable operation for 100 minutes. In contrast, here, a record-low EEC of 84.9 $\text{kJ mol}^{-1} \text{CO}_2$ was achieved, while maintaining operational stability for up to four hours, representing a 19% reduction in energy consumption. Moreover, this study revealed the future challenges of utilizing RSW on the EHL performance, for the first time. This led to several critical challenges being identified for specific reactor components, such as the sodium exchange membrane and cathode. Finally, a preliminary mitigation strategy was proposed to assess the feasibility of overcoming these challenges and to enable longer operation (10 h) which allowed to assess whether RSW utilization would lead to other consequences and challenges hampering real world application of the EHL system. While the current density in this study remained limited to a maximum of 10 mA cm^{-2} and the previous study of Yan *et al.* tested up to 40 mA cm^{-2} , invaluable insights were gained concerning the challenges of using realistic seawater. Therefore, future research should focus on scaling up the system to achieve industrially relevant current densities approaching 1 A cm^{-2} , which are relevant for real world applications. Nevertheless, the primary objective was to evaluate the feasibility of the EHL technology under exposure to RSW. Correspondingly, lower current densities were employed to explore this under-investigated aspect of the EHL technology, to unravel future challenges and to gain insights into whether they can be mitigated. Furthermore, this indirect ocean capture technology offers a viable alternative to BPMED and E-CEM, both of which commonly require IrO_2 catalysts, thereby contributing to resource depletion. Notably, the EHL

technology is inherently self-sustaining, requiring only a minimal amount of hydrogen to initiate operation.

4. Conclusion

This work aimed to investigate the feasibility of the electrochemical hydrogen looping system to capture carbon dioxide from seawater under real world conditions. The findings presented in this manuscript provide more insight into the electrochemical energy consumption of the relatively new EHL technology and the challenges that occur when realistic seawater is employed as an electrolyte for the first time.

To benchmark our EHL setup compared to previously reported research, synthetic seawater was utilized. These results demonstrated that our cell operates with a 25% reduction in cell potential relative to the best-performing system reported in the literature.¹⁹ This optimal working point was the result of a parameter study, varying the current density and SSW flow rate to achieve an EEC of 77.5 kJ mol⁻¹ CO₂, recorded at a flow rate of 15 mL min⁻¹ and a current density of 2 mA cm⁻².

Subsequently, the EHL system was subjected to the utilization of realistic seawater, introducing additional ions and thereby identifying some of the challenges that this technology will face under real world conditions to, ultimately, become industrially feasible. Here, the anticipated issue of salt formation, inherent to the characteristics of the technology was confirmed, giving rise to salt precipitation on the platinum cathode, in the cathodic flow field, and on/in the membranes. SEM-EDS measurements illustrated the latter on a microscopic level and additional chronopotentiometry experiments established the magnitude of membrane scaling, which resulted in an elevated cell voltage after only one hour of operation. Still, a record-low EEC of 100.8 kJ mol⁻¹ CO₂ was documented at a current density of 5 mA cm⁻² while employing a RSW flow rate of 25 mL min⁻¹ in both the middle and cathodic compartment.

Finally, the issue of salt precipitation and membrane scaling was addressed with the introduction of an *in situ* acidic wash step, during which the cathodic and middle compartments were periodically washed using an aqueous HCl solution. After preliminary optimization of this mitigation strategy, an increase in performance during long-term operation was recorded. Consequently, the cell voltage increased by only 0.106 ± 0.004 V over 10 hours of operation while without mitigation an increase of 0.191 ± 0.026 V was already recorded after four hours of operation. The former was established when performing a wash step with 0.5 M HCl at 45 mL min⁻¹ for 10 minutes every hour while operating the reactor at 5 mA cm⁻² with a RSW flow rate of 25 mL min⁻¹.

While these results emphasize the potential of this young technology for industrial oceanic carbon capture and utilization, further optimization to counter salt precipitation and membrane scaling remain necessary. Especially looking toward real world application at industrially relevant current densities, the necessity for a reliable and green mitigation

strategy only increases. Together with electrochemical reactor engineering, for example by developing thinner spacers to further reduce the cell resistance and corresponding electrochemical energy consumption and the development of improved membranes, have the potential to make the electrochemical hydrogen looping system even more sustainable and to advance this young technology toward real world industrial application.

Data availability

The (processed) data will be published and made openly and freely available through deposition in the Zenodo repository of the University of Antwerp and Applied Electrochemistry and Catalysis (ELCAT) Research Group. <https://zenodo.org/communities/uantwerp-elcat/>.

Conflicts of interest

The authors declare no conflicts of interest.

Acknowledgements

The authors would like to dedicate this work to the memory of lab expert Ing. Thomas Kenis, whose invaluable knowledge and assistance contributed immensely to this work. The authors would like to thank BASF for providing funding for the experimental work (48675). Furthermore, the authors would like to thank the EMAT research group (University of Antwerp) for providing the necessary equipment and knowledge for the SEM EDS measurements.

References

- 1 A. Dubey and A. Arora, *J. Cleaner Prod.*, 2022, **373**, 133932.
- 2 F. M. Baena-Moreno, M. Rodríguez-Galán, F. Vega, B. Alonso-Fariñas, L. F. Vilches Arenas and B. Navarrete, *Energy Sources, Part A*, 2019, **41**, 1403–1433.
- 3 T. Wilberforce, A. G. Olabi, E. T. Sayed, K. Elsaid and M. A. Abdelkareem, *Sci. Total Environ.*, 2021, **761**, 143203.
- 4 A. Bhavsar, D. Hingar, S. Ostwal, I. Thakkar, S. Jadeja and M. Shah, *Case Stud. Chem. Environ. Eng.*, 2023, **8**, 100368.
- 5 J. S. Kikstra, Z. R. Nicholls, C. J. Smith, J. Lewis, R. D. Lamboll, E. Byers, M. Sandstad, M. Meinshausen, M. J. Gidden and J. Rogelj, *Geosci. Model Dev.*, 2022, **15**, 9075–9109.
- 6 UNFCCC, The Paris Agreement 2015.
- 7 J. F. D. Tapia, J.-Y. Lee, R. E. H. Ooi, D. C. Y. Foo and R. R. Tan, *Sustainable Prod. Consum.*, 2018, **13**, 1–15.
- 8 F. Nocito and A. Dibenedetto, *Curr. Opin. Green Sustain. Chem.*, 2020, **21**, 34–43.
- 9 D. W. Keith, G. Holmes, D. S. Angelo and K. Heidel, *Joule*, 2018, **2**, 1573–1594.

- 10 K. S. Lackner, S. Brennan, J. M. Matter, A.-H. A. Park, A. Wright and B. Van Der Zwaan, *Proc. Natl. Acad. Sci. U. S. A.*, 2012, **109**, 13156–13162.
- 11 C.-F. de Lannoy, M. D. Eisaman, A. Jose, S. D. Karnitz, R. W. DeVaul, K. Hannun and J. L. B. Rivest, *Int. J. Greenhouse Gas Control*, 2018, **70**, 243–253.
- 12 M. D. Eisaman, J. L. B. Rivest, S. D. Karnitz, C.-F. de Lannoy, A. Jose, R. W. DeVaul and K. Hannun, *Int. J. Greenhouse Gas Control*, 2018, **70**, 254–261.
- 13 Climeworks, Climeworks switches on world's largest direct air capture plant, <https://climeworks.com/press-release/climeworks-switches-on-worlds-largest-direct-air-capture-plant-mammoth>.
- 14 C. Beuttler, L. Charles and J. Wurzbacher, *Front. Clim.*, 2019, **1**, 10.
- 15 H. D. Willauer, F. DiMascio, D. R. Hardy and F. W. Williams, *Ind. Eng. Chem. Res.*, 2014, **53**, 12192–12200.
- 16 T. Coffey, D. R. Hardy, G. E. Besenbruch, K. R. Schultz, L. C. Brown and J. P. Dahlburg, *Def. Horiz.*, 2003, 1–11.
- 17 R. E. Zeebe, *Annu. Rev. Earth Planet. Sci.*, 2012, **40**, 141–165.
- 18 R. Sharifian, L. Boer, R. Wagterveld and D. Vermaas, *Chem. Eng. J.*, 2022, **438**, 135326.
- 19 L. Yan, J. Bao, Y. Shao and W. Wang, *ACS Energy Lett.*, 2022, **7**, 1947–1952.
- 20 M. D. Eisaman, L. Alvarado, D. Larner, P. Wang, B. Garg and K. A. Littau, *Energy Environ. Sci.*, 2011, **4**, 1319–1328.
- 21 H. D. Willauer, F. DiMascio, D. R. Hardy, M. K. Lewis and F. W. Williams, *Ind. Eng. Chem. Res.*, 2011, **50**, 9876–9882.
- 22 J. Zhang, H. Li, Z. Shi and J. Zhang, *Int. J. Green Energy*, 2010, **7**, 461–474.
- 23 Y. Chen, F. Mojica, G. Li and P. Y. A. Chuang, *Int. J. Energy Res.*, 2017, **41**, 2365–2373.
- 24 M. Khan, T. Al-Attas, S. Roy, M. M. Rahman, N. Ghaffour, V. Thangadurai, S. Larter, J. Hu, P. M. Ajayan and M. G. Kibria, *Energy Environ. Sci.*, 2021, **14**, 4831–4839.
- 25 M. D. Eisaman, K. Parajuly, A. Tuganov, C. Eldershaw, N. Chang and K. A. Littau, *Energy Environ. Sci.*, 2012, **5**, 7346–7352.
- 26 H. D. Willauer, F. DiMascio, D. R. Hardy and F. W. Williams, *Energy Fuels*, 2017, **31**, 1723–1730.
- 27 W. Wang, M. Hu, Y. Zheng, P. Wang and C. Ma, *Ind. Eng. Chem. Res.*, 2011, **50**, 8333–8339.
- 28 I. A. Digdaya, I. Sullivan, M. Lin, L. Han, W.-H. Cheng, H. A. Atwater and C. Xiang, *Nat. Commun.*, 2020, **11**, 4412.
- 29 T. Luo, S. Abdu and M. Wessling, *J. Membr. Sci.*, 2018, **555**, 429–454.
- 30 B. M. Dobyys, J. M. Kim, J. Li, Z. Jiang and B. S. Beckingham, *Polymer*, 2020, **209**, 123046.
- 31 S. Mikhaylin and L. Bazinet, *Adv. Colloid Interface Sci.*, 2016, **229**, 34–56.